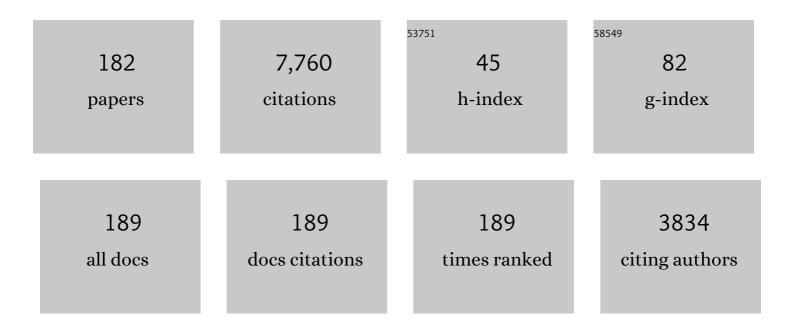
## Weidong Sun

List of Publications by Year in descending order

Source: https://exaly.com/author-pdf/6669525/publications.pdf Version: 2024-02-01



#	Article	IF	CITATIONS
1	Geochemistry and genesis of the Nadun Nb-enriched arc basalt in the Duolong mineral district, western Tibet: Indication of ridge subduction. Geoscience Frontiers, 2022, 13, 101283.	4.3	8
2	A Spectral–Spatial Jointed Spectral Super-Resolution and Its Application to HJ-1A Satellite Images. IEEE Geoscience and Remote Sensing Letters, 2022, 19, 1-5.	1.4	7
3	Spectral Anomaly Detection Based on Dictionary Learning for Sea Surfaces. IEEE Geoscience and Remote Sensing Letters, 2022, 19, 1-5.	1.4	2
4	The Rotation of the Pacific Plate Induced by the Ontong Java Large Igneous Province. Journal of Earth Science (Wuhan, China), 2022, 33, 544-551.	1.1	7
5	Large iron isotope fractionation during mantle wedge serpentinization: Implications for iron isotopes of arc magmas. Earth and Planetary Science Letters, 2022, 583, 117423.	1.8	11
6	Reply to "Is 'plume interaction induced migration of the hawaiian-emperor seamounts' a step too far?― Science Bulletin, 2022, 67, 1221-1221.	4.3	0
7	Incremental Dictionary Learning for Multiframe Satellite Image Representation via Gradual Optimization. IEEE Transactions on Geoscience and Remote Sensing, 2022, 60, 1-16.	2.7	4
8	Data Augmentation Using Bitplane Information Recombination Model. IEEE Transactions on Image Processing, 2022, 31, 3713-3725.	6.0	3
9	Preface: Pacific Plate Subduction and the Yanshanian Movement in Eastern China. Journal of Earth Science (Wuhan, China), 2022, 33, 541-543.	1.1	5
10	Geochemical and Zircon Hf-O Isotopic Constraints on the Origin of Wulian A-Type Granite in Shandong Peninsula, Eastern China. Journal of Earth Science (Wuhan, China), 2022, 33, 609-622.	1.1	3
11	Effect of F-Rich Fluids on the A-Type Magmatism and Related Metal Mobilization: New Insights from the Fogang-Nankunshan-Yajishan Igneous Rocks in Southeast China. Journal of Earth Science (Wuhan,) Tj ETQq1 1	0.784314	rgB∏ /Overloo
12	Pluton incremental growth by multi-stage magma pulsations: Evidence from the Fangshan pluton, North China Craton. Tectonophysics, 2022, 838, 229480.	0.9	1
13	Three late-Mesozoic fluorite deposit belts in southeast China and links to subduction of the (paleo-) Pacific plate. Ore Geology Reviews, 2021, 129, 103865.	1.1	11
14	Investigation of an oceanic plateau formation and rifting initiation model implied by the Caroline Ridge on the Caroline Plate, western Pacific. International Geology Review, 2021, 63, 193-207.	1.1	9
15	The big mantle wedge and decratonic gold deposits. Science China Earth Sciences, 2021, 64, 1451-1462.	2.3	36
16	Boron, arsenic and antimony recycling in subduction zones: New insights from interactions between forearc serpentinites and CO2-rich fluids at the slab-mantle interface. Geochimica Et Cosmochimica Acta, 2021, 298, 21-42.	1.6	9
17	Plume-ridge interaction induced migration of the Hawaiian-Emperor seamounts. Science Bulletin, 2021,	4.3	18
18	MORB-like δ56Fe values unveil the effect of subduction on the South China Sea basalts. Chemical Geology, 2021, 569, 120124.	1.4	8

#	Article	IF	CITATIONS
19	Experimental constraints on trace element partitioning between coesite and hydrous silicate melt at 5 GPa and 1500–1750°C. Science China Earth Sciences, 2021, 64, 1171-1183.	2.3	2
20	Calcium isotopic fractionation during magma differentiation: Constraints from volcanic glasses from the eastern Manus Basin. Geochimica Et Cosmochimica Acta, 2021, 305, 228-242.	1.6	16
21	Contrasted Effect of Spinel and Pyroxene on Molecular Hydrogen (H2) Production during Serpentinization of Olivine. Minerals (Basel, Switzerland), 2021, 11, 794.	0.8	3
22	Genesis and mineralization potential of the Late Cretaceous Chemen granodioritic intrusion in the southern Gangdese magmatic belt, Tibet. Journal of Asian Earth Sciences, 2021, 217, 104829.	1.0	6
23	Plate subduction, oxygen fugacity, and mineralization. Journal of Oceanology and Limnology, 2020, 38, 64-74.	0.6	31
24	High oxygen fugacity magma: implication for the destruction of the North China Craton. Acta Geochimica, 2020, 39, 161-171.	0.7	13
25	Calcium isotopic fractionation during plate subduction: Constraints from back-arc basin basalts. Geochimica Et Cosmochimica Acta, 2020, 270, 379-393.	1.6	29
26	Occurrence of Halogenated Organic Pollutants in Hadal Trenches of the Western Pacific Ocean. Environmental Science & Technology, 2020, 54, 15821-15828.	4.6	36
27	Plate convergence in the Indo-Pacific region. Journal of Oceanology and Limnology, 2020, 38, 1008-1017.	0.6	18
28	Blind Super-Resolution for Single Remote Sensing Image via Sparse Representation and Transformed Self-Similarity. Journal of Physics: Conference Series, 2020, 1575, 012115.	0.3	2
29	Evaluation of a deep learningâ€based computerâ€aided diagnosis system for distinguishing benign from malignant thyroid nodules in ultrasound images. Medical Physics, 2020, 47, 3952-3960.	1.6	31
30	An Efficient Compression Method of Hyperspectral Images Based on Compressed Sensing and Joint Optimization. Integrated Ferroelectrics, 2020, 208, 194-205.	0.3	0
31	Calcium isotopic signatures of depleted mid-ocean ridge basalts from the northeastern Pacific. Journal of Oceanology and Limnology, 2020, 38, 1476-1487.	0.6	7
32	The formation of the giant Huayangchuan U-Nb deposit associated with carbonatite in the Qingling Orogenic Belt. Ore Geology Reviews, 2020, 122, 103498.	1.1	27
33	An Efficient Method of Hyperspectral Image Dimension Reduction Based on Low Rank Representation and Locally Linear Embedding. Integrated Ferroelectrics, 2020, 208, 206-214.	0.3	2
34	Early cretaceous transformation from Pacific to Neo-Tethys subduction in the SW Pacific Ocean: Constraints from Pb-Sr-Nd-Hf isotopes of the Philippine arc. Geochimica Et Cosmochimica Acta, 2020, 285, 21-40.	1.6	15
35	"Yanshanian Movement―induced by the westward subduction of the paleo–Pacific plate. Solid Earth Sciences, 2020, 5, 103-114.	0.8	22
36	Effect of pressure on the kinetics of peridotite serpentinization. Physics and Chemistry of Minerals, 2020, 47, 1.	0.3	10

#	Article	IF	CITATIONS
37	Geochemistry of pyrite from stratabound massive sulfide deposits, Tongling region, China: Implication for their genesis. Ore Geology Reviews, 2020, 120, 103430.	1.1	17
38	Hyperspectral and Multispectral Image Fusion Using Optimized Twin Dictionaries. IEEE Transactions on Image Processing, 2020, 29, 4709-4720.	6.0	32
39	Geochemistry of sulfide minerals from skarn Cu (Au) deposits in the Fenghuangshan ore field, Tongling, eastern China: Insights into ore-forming process. Ore Geology Reviews, 2020, 122, 103537.	1.1	17
40	Geochronology and geochemistry of the Late Cretaceous Xinpeng granitic intrusion, South China: Implication for Sn-W mineralization. Ore Geology Reviews, 2019, 113, 103075.	1.1	18
41	New discrimination diagrams for basalts based on big data research. Big Earth Data, 2019, 3, 45-55.	2.0	12
42	The Magma Engine and subduction initiation. Acta Geochimica, 2019, 38, 611-612.	0.7	5
43	Rhenium enrichment in the northwest Pacific arc. Ore Geology Reviews, 2019, 115, 103176.	1.1	9
44	Thyroid Nodule Detection in Ultrasound Images with Convolutional Neural Networks. , 2019, , .		10
45	Automated detection and classification of thyroid nodules in ultrasound images using clinical-knowledge-guided convolutional neural networks. Medical Image Analysis, 2019, 58, 101555.	7.0	131
46	Hyperspectral and Multispectral Image Fusion Using Cluster-Based Multi-Branch BP Neural Networks. Remote Sensing, 2019, 11, 1173.	1.8	33
47	Early Cretaceous adakite from the Atlas porphyry Cu-Au deposit in Cebu Island, Central Philippines: Partial melting of subducted oceanic crust. Ore Geology Reviews, 2019, 110, 102937.	1.1	32
48	Comparative geochemical study of scheelite from the Shizhuyuan and Xianglushan tungsten skarn deposits, South China: Implications for scheelite mineralization. Ore Geology Reviews, 2019, 109, 448-464.	1.1	36
49	Geochronological and geochemical constraints on the formation of Chizhou Cu-Mo polymetallic deposits, middle and lower Yangtze metallogenic belt, eastern China. Ore Geology Reviews, 2019, 109, 322-347.	1.1	23
50	A new model for porphyry W mineralization in a world-class tungsten metallogenic belt. Ore Geology Reviews, 2019, 107, 501-512.	1.1	18
51	Influence of pH on Molecular Hydrogen (H2) Generation and Reaction Rates during Serpentinization of Peridotite and Olivine. Minerals (Basel, Switzerland), 2019, 9, 661.	0.8	9
52	The Late Mesozoic granodiorite and polymetallic mineralization in southern Anhui Province, China: A perspective from apatite geochemistry. Solid Earth Sciences, 2019, 4, 178-189.	0.8	20
53	Reconstruction From Multispectral to Hyperspectral Image Using Spectral Library-Based Dictionary Learning. IEEE Transactions on Geoscience and Remote Sensing, 2019, 57, 1325-1335.	2.7	19
54	Source of ore-forming fluids of the Yangshan gold field, western Qinling orogen, China: Evidence from microthermometry, noble gas isotopes and in situ sulfur isotopes of Au-carrying pyrite. Ore Geology Reviews, 2019, 105, 404-422.	1.1	28

#	Article	IF	CITATIONS
55	Geochemical constraints on genesis of Paleoproterozoic A-type granite in the south margin of North China Craton. Lithos, 2018, 304-307, 489-500.	0.6	29
56	Calcium Isotopic Compositions of Normal Midâ€Ocean Ridge Basalts From the Southern Juan de Fuca Ridge. Journal of Geophysical Research: Solid Earth, 2018, 123, 1303-1313.	1.4	53
57	Crystal fractionation of granitic magma during its non-transport processes: A physics-based perspective. Science China Earth Sciences, 2018, 61, 190-204.	2.3	15
58	Origin of Early Cretaceous Guandian adakitic pluton in central eastern China: partial melting of delaminated lower continental crust triggered by ridge subduction. International Geology Review, 2018, 60, 1707-1720.	1.1	9
59	Petrogenesis and metallogenic implications of Late Mesozoic intrusive rocks in the Tongling region, eastern China: a case study and perspective review. International Geology Review, 2018, 60, 1361-1380.	1.1	35
60	Palaeoarchaean materials in the Tibetan Plateau indicated by zircon. International Geology Review, 2018, 60, 1061-1072.	1.1	8
61	Early Cretaceous adakitic rocks in the Anqing region, southeastern China: constraints on petrogenesis and metallogenic significance. International Geology Review, 2018, 60, 1435-1452.	1.1	25
62	Spectral Super-resolution for RGB Images using Class-based BP Neural Networks. , 2018, , .		10
63	Jurassic and Cretaceous (Yanshannian) tectonics, magmatism and metallogenesis in South China: preface. International Geology Review, 2018, 60, 1321-1325.	1.1	7
64	Fluids, Metals, and Mineral/Ore Deposits. Geofluids, 2018, 2018, 1-6.	0.3	13
65	Meltâ€Fluxed Melting of the Heterogeneously Mixed Lower Arc Crust: A Case Study from the Qinling Orogenic Belt, Central China. Geochemistry, Geophysics, Geosystems, 2018, 19, 1767-1788.	1.0	15
66	Thermodynamic and Elastic Properties of Magnesite at Mantle Conditions: Firstâ€Principles Calculations. Geochemistry, Geophysics, Geosystems, 2018, 19, 2719-2731.	1.0	16
67	Recycling of subducted upper continental crust: Constraints on the extensive molybdenum mineralization in the Qinling–Dabie orogen. Ore Geology Reviews, 2017, 81, 451-465.	1.1	41
68	The production of iron oxide during peridotite serpentinization: Influence of pyroxene. Geoscience Frontiers, 2017, 8, 1311-1321.	4.3	28
69	Adakitic rocks associated with the Shilu copper–molybdenum deposit in the Yangchun Basin, South China, and their tectonic implications. Acta Geochimica, 2017, 36, 132-150.	0.7	55
70	Petrogenesis and tectonic implications of late Mesozoic granitoids in southern Anhui Province, southeastern China. International Geology Review, 2017, 59, 1804-1826.	1.1	29
71	Early Cretaceous high-Mg adakites associated with Cu-Au mineralization in the Cebu Island, Central Philippines: Implication for partial melting of the paleo-Pacific Plate. Ore Geology Reviews, 2017, 88, 251-269.	1.1	19
72	Influence of temperature, pressure, and fluid salinity on the distribution of chlorine into serpentine minerals. Journal of Asian Earth Sciences, 2017, 145, 101-110.	1.0	11

#	Article	IF	CITATIONS
73	Feature Extraction for Hyperspectral Images Using Low-Rank Representation With Neighborhood Preserving Regularization. IEEE Geoscience and Remote Sensing Letters, 2017, 14, 836-840.	1.4	10
74	Deep carbon cycles constrained by a large-scale mantle Mg isotope anomaly in eastern China. National Science Review, 2017, 4, 111-120.	4.6	240
75	The formation of the Late Cretaceous Xishan Sn–W deposit, South China: Geochronological and geochemical perspectives. Lithos, 2017, 290-291, 253-268.	0.6	60
76	Nanosecond laser ablation tandem inductively coupled plasma mass and optical emission spectrometry for micro-chemical elemental analysis. Journal of Analytical Atomic Spectrometry, 2017, 32, 2246-2253.	1.6	1
77	Distinguishing Cloud and Snow in Satellite Images via Deep Convolutional Network. IEEE Geoscience and Remote Sensing Letters, 2017, 14, 1785-1789.	1.4	89
78	Major transition of continental basalts in the Early Cretaceous: Implications for the destruction of the North China Craton. Chemical Geology, 2017, 470, 93-106.	1.4	51
79	Marine Carbonate Component in the Mantle Beneath the Southeastern Tibetan Plateau: Evidence From Magnesium and Calcium Isotopes. Journal of Geophysical Research: Solid Earth, 2017, 122, 9729-9744.	1.4	60
80	The initiation of plate subduction. Solid Earth Sciences, 2017, 2, 89-90.	0.8	5
81	Blind image deblurring based on sparse representation and structural self-similarity. , 2017, , .		5
82	Feature selection and thyroid nodule classification using transfer learning. , 2017, , .		16
83	Unsupervised feature extraction for hyperspectral images using combined low rank representation and locally linear embedding. , 2017, , .		7
84	Classification of thyroid nodules in ultrasound images using deep model based transfer learning and hybrid features. , 2017, , .		59
85	The formation of porphyry copper deposits. Acta Geochimica, 2017, 36, 9-15.	0.7	71
86	LRR-based hyperspectral image restoration by exploiting the union structure of spectral space and with robust dictionary estimation. , 2017, , .		2
87	Influence of pyroxene and spinel on the kinetics of peridotite serpentinization. Journal of Geophysical Research: Solid Earth, 2017, 122, 7111-7126.	1.4	23
88	Hyperspectral image super-resolution based on non-factorization sparse representation and dictionary learning. , 2017, , .		1
89	Hyperspectral image fusion based on non-factorization sparse representation and error matrix estimation. , 2017, , .		3
90	Hyperspectral Image Denoising Based on Subspace Low Rank Representation. Communications in Computer and Information Science, 2017, , 51-59.	0.4	1

#	Article	IF	CITATIONS
91	Partial melting of subducted paleo-Pacific plate during the early Cretaceous: Constraint from adakitic rocks in the Shaxi porphyry Cu–Au deposit, Lower Yangtze River Belt. Lithos, 2016, 262, 651-667.	0.6	78
92	Generation of Late Mesozoic Qianlishan A 2 -type granite in Nanling Range, South China: Implications for Shizhuyuan W–Sn mineralization and tectonic evolution. Lithos, 2016, 266-267, 435-452.	0.6	130
93	Ship wake detection for SAR images with complex backgrounds based on morphological dictionary learning. , 2016, , .		7
94	Initiation and evolution of the South China Sea: an overview. Acta Geochimica, 2016, 35, 215-225.	0.7	88
95	Denoising of Hyperspectral Images Using Group Low-Rank Representation. IEEE Journal of Selected Topics in Applied Earth Observations and Remote Sensing, 2016, 9, 4420-4427.	2.3	55
96	Subduction and ore deposits. International Geology Review, 2015, 57, iii-vi.	1.1	16
97	A spectral unmixing method based on wavelet weighted similarity. , 2015, , .		2
98	Olivine versus peridotite during serpentinization: Gas formation. Science China Earth Sciences, 2015, 58, 2165-2174.	2.3	16
99	Automatic analysis of the slight change image for unsupervised change detection. Journal of Applied Remote Sensing, 2015, 9, 095995.	0.6	7
100	Group-based hyperspectral image denoising using low rank representation. , 2015, , .		11
101	The Lamandau IOCG deposit, southwestern Kalimantan Island, Indonesia: Evidence for its formation from geochronology, mineralogy, and petrogenesis of igneous host rocks. Ore Geology Reviews, 2015, 68, 43-58.	1.1	8
102	Slab break-off model for the Triassic syn-collisional granites in the Qinling orogenic belt, Central China: Zircon U-Pb age and Hf isotope constraints. International Geology Review, 2015, 57, 492-507.	1.1	31
103	Decratonic gold deposits: a new concept and new opportunities. National Science Review, 2015, 2, 248-249.	4.6	11
104	Porphyry deposits and oxidized magmas. Ore Geology Reviews, 2015, 65, 97-131.	1.1	420
105	Super-resolution hyperspectral imaging with unknown blurring by low-rank and group-sparse modeling. , 2014, , .		12
106	Super-resolution mapping via multi-dictionary based sparse representation. , 2014, , .		33
107	Mineralogical study of sediment-hosted gold deposits in the Yangshan ore field, Western Qinling Orogen, Central China. Journal of Asian Earth Sciences, 2014, 85, 40-52.	1.0	19
108	Partitioning of copper between olivine, orthopyroxene, clinopyroxene, spinel, garnet and silicate melts at upper mantle conditions. Geochimica Et Cosmochimica Acta, 2014, 125, 1-22.	1.6	87

#	Article	IF	CITATIONS
109	Superresolution Mapping Using Multiple Dictionaries by Sparse Representation. IEEE Geoscience and Remote Sensing Letters, 2014, 11, 2055-2059.	1.4	9
110	The Permian–Triassic granitoids in Bayan Obo, North China Craton: A geochemical and geochronological study. Lithos, 2014, 190-191, 430-439.	0.6	46
111	Petrogenesis and mineralization of the Fenghuangshan skarn Cu–Au deposit, Tongling ore cluster field, Lower Yangtze metallogenic belt. Ore Geology Reviews, 2014, 58, 148-162.	1.1	56
112	Geochronological and geochemical constraints on genesis of the adakitic rocks in Outang, South Tan–Lu Fault Belt (Northeastern Yangtze Block). Tectonophysics, 2014, 626, 86-104.	0.9	31
113	Super-Resolution Based on Compressive Sensing and Structural Self-Similarity for Remote Sensing Images. IEEE Transactions on Geoscience and Remote Sensing, 2013, 51, 4864-4876.	2.7	113
114	U-Pb and Re-Os Geochronology of the Tongcun Molybdenum Deposit and Zhilingtou Gold-Silver Deposit in Zhejiang Province, Southeast China, and Its Geological Implications. Resource Geology, 2013, 63, 99-109.	0.3	29
115	Major Nb/Ta Fractionation Recorded in Garnet Amphibolite Facies Metagabbro. Journal of Geology, 2013, 121, 255-274.	0.7	38
116	Destruction of the North China Craton Induced by Ridge Subductions. Journal of Geology, 2013, 121, 197-213.	0.7	88
117	Large-scale gold mineralization in eastern China induced by an Early Cretaceous clockwise change in Pacific plate motions. International Geology Review, 2013, 55, 311-321.	1.1	71
118	Geochemical studies on Permian manganese deposits in Guichi, eastern China: Implications for their origin and formative environments. Journal of Asian Earth Sciences, 2013, 74, 155-166.	1.0	20
119	A Small and Lightweight Autonomous Laser Mapping System without GPS. Journal of Field Robotics, 2013, 30, 784-802.	3.2	10
120	Petrology, geochemistry, and tectonic significance of Mesozoic shoshonitic volcanic rocks, Luzong volcanic basin, eastern China. International Geology Review, 2012, 54, 714-736.	1.1	53
121	The genetic association of adakites and Cu–Au ore deposits': a reply. International Geology Review, 2012, 54, 370-372.	1.1	16
122	The formation of the Dabaoshan porphyry molybdenum deposit induced by slab rollback. Lithos, 2012, 150, 101-110.	0.6	183
123	Early Cretaceous dioritic rocks in the Tongling region, eastern China: Implications for the tectonic settings. Lithos, 2012, 150, 49-61.	0.6	89
124	Indosinian isotope ages of plutons and deposits in southwestern Miaoershan-Yuechengling, northeastern Guangxi and implications on Indosinian mineralization in South China. Science Bulletin, 2012, 57, 1024-1035.	1.7	58
125	Mesozoic large magmatic events and mineralization in SE China: oblique subduction of the Pacific plate. International Geology Review, 2011, 53, 704-726.	1.1	178
126	The genetic association of adakites and Cu–Au ore deposits. International Geology Review, 2011, 53, 691-703.	1.1	202

4

#	Article	IF	CITATIONS
127	Different origins of adakites from the Dabie Mountains and the Lower Yangtze River Belt, eastern China: geochemical constraints. International Geology Review, 2011, 53, 727-740.	1.1	123
128	Partitioning of Nb and Ta between rutile and felsic melt and the fractionation of Nb/Ta during partial melting of hydrous metabasalt. Geochimica Et Cosmochimica Acta, 2011, 75, 1673-1692.	1.6	143
129	Exhumation of the Dahinggan Mountains, NE China from the Late Mesozoic to the Cenozoic: New evidence from fission-track thermochronology. Journal of Asian Earth Sciences, 2011, 42, 123-133.	1.0	33
130	Super resolution of remote sensing image based on structure similarity in CS frame. Proceedings of SPIE, 2011, , .	0.8	1
131	A mosaic approach for unmanned airship remote sensing images based on compressive sensing. Proceedings of SPIE, 2011, , .	0.8	0
132	Geochronology of the Xihuashan Tungsten Deposit in Southeastern China: Constraints from Re–Os and U–Pb Dating. Resource Geology, 2011, 61, 414-423.	0.3	40
133	Zircon U-Pb ages of granites at Changba and Huangzhuguan in western Qinling and implications for source nature. Science Bulletin, 2011, 56, 659-669.	1.7	22
134	A graph cuts based human shadow extraction using entropy-expressed texture and color features. , 2011, , .		0
135	Channelized fluids in subducted continental crust: constraints from ÎƊ–δ180 of quartz and fluid inclusions in quartz veins from the Chinese Continental Scientific Drilling Project. International Geology Review, 2011, 53, 1443-1463.	1.1	2
136	Geochemical and zircon U–Pb study of the Huangmeijian A-type granite: implications for geological evolution of the Lower Yangtze River belt. International Geology Review, 2011, 53, 499-525.	1.1	90
137	The fluxes and controlling factors of N2O and CH4 emissions from freshwater marsh in Northeast China. Science China Earth Sciences, 2010, 53, 700-709.	2.3	8
138	Ridge subduction and porphyry copper-gold mineralization: An overview. Science China Earth Sciences, 2010, 53, 475-484.	2.3	264
139	Emplacement age of the Songshugou ultramafic massif in the Qinling orogenic belt, and geologic implications. International Geology Review, 2009, 51, 58-76.	1.1	29
140	Geochronological and geochemical constraints on formation of the Tongling metal deposits, middle Yangtze metallogenic belt, eastâ€central China. International Geology Review, 2009, 51, 388-421.	1.1	98
141	The genesis of sandstoneâ€type uranium deposits in the Ordos Basin, NW China: constraints provided by fluid inclusions and stable isotopes. International Geology Review, 2009, 51, 422-455.	1.1	36
142	The Application of Data Fitting in Direct Geolocation of Remote Sensing Data. , 2009, , .		0
143	Geology, geochemistry, and genesis of Axi: A Paleozoic low-sulfidation type epithermal gold deposit in Xinjiang, China. Ore Geology Reviews, 2009, 36, 265-281.	1.1	101

144 Finding all the solutions of PnP problem. , 2009, , .

# ARTICLE IF CITATIONS Natural and experimental constraints on formation of the continental crust based on 145 1.1 niobiumâ€"tantalum fractionation. International Geology Review, 2009, 51, 473-501. A new optimal seam selection method for airborne image stitching., 2009, , . 146 9 Experimental constraints on rutile saturation during partial melting of metabasalt at the amphibolite 86 to eclogite transition, with applications to TTG genesis. American Mineralogist, 2009, 94, 1175-1186. PGE geochemistry and Re–Os dating of massive sulfide ores from the Baimazhai Cu–Ni deposit, Yunnan 148 0.6 28 province, China. Lithos, 2008, 105, 12-24. Biogenic nitric oxide emission from saline sodic soils in a semiarid region, northeastern China: A 149 3.3 18 laboratory study. Journal of Geophysical Research, 2008, 113, . 150 Constancy of Nb/U in the mantle revisited. Geochimica Et Cosmochimica Acta, 2008, 72, 3542-3549. 90 1.6 Minimum distance constrained non-negative matrix factorization for the endmember extraction of 0.8 hyperspectral images. Proceedings of SPIE, 2007, , . New sub-pixel unmixing method based on blind signal separation. Proceedings of SPIE, 2007, , . 152 0.8 0 Combined contextual classification method for large scale land covering based on multi-resolution satellite data., 2007,,. The golden transformation of the Cretaceous plate subduction in the west Pacific. Earth and 154 1.8 666 Planetary Science Letters, 2007, 262, 533-542. Monazite, iron oxide and barite exsolutions in apatite aggregates from CCSD drillhole eclogites and 1.6 their geological implications. Geochimica Et Cosmochimica Acta, 2007, 71, 2896-2905. Enhanced net formations of nitrous oxide and methane underneath the frozen soil in Sanjiang 156 3.3 27 wetland, northeastern China. Journal of Geophysical Research, 2007, 112, . Making continental crust through slab melting: Constraints from niobium–tantalum fractionation in 1.6 111 UHP metamorphic rutile. Geochimica Et Cosmochimica Acta, 2006, 70, 4770-4782. Study on the Geolocation Algorithm of Space-Borne SAR Image. Lecture Notes in Computer Science, 158 1.0 7 2006, , 270-280. Release of gold-bearing fluids in convergent margin magmas prompted by magnetite crystallization. Nature, 2004, 431, 975-978. The mechanism of Re enrichment in arc magmas: evidence from Lau Basin basaltic glasses and primitive 160 1.8 75 melt inclusions. Earth and Planetary Science Letters, 2004, 222, 101-114. Enhanced mantle-to-crust rhenium transfer in undegassed arc magmas. Nature, 2003, 422, 294-297. 161 13.7 131 Reâ€Os Dating of Sulfides from the Volcanogenic Massive Sulfide Deposit at Gacun, Southwestern 162 0.3 13 China. Resource Geology, 2003, 53, 305-310.

#	Article	IF	CITATIONS
163	Evidence for rhenium enrichment in the mantle wedge from submarine arc–like volcanic glasses (Papua New Guinea). Geology, 2003, 31, 845.	2.0	76
164	Timing of Synorogenic Granitoids in the South Qinling, Central China: Constraints on the Evolution of the Qinlingâ€Ðabie Orogenic Belt. Journal of Geology, 2002, 110, 457-468.	0.7	216
165	Mid-paleozoic collision in the north Qinling: Sm–Nd, Rb–Sr and 40 Ar/ 39 Ar ages and their tectonic implications. Journal of Asian Earth Sciences, 2002, 21, 69-76.	1.0	100
166	Carboniferous and Triassic eclogites in the western Dabie Mountains, east-central China: evidence for protracted convergence of the North and South China Blocks. Journal of Metamorphic Geology, 2002, 20, 873-886.	1.6	182
167	Nd isotopic disequilibrium between minerals and Rb-Sr age of the secondary phengite in eclogite from the Yangkou area, Qingdao, eastern China. Science Bulletin, 2001, 46, 252-255.	1.7	8
168	Re-Os isotopic composition of the Dongling IIICD iron meteorite. Science Bulletin, 2001, 46, 518-520.	1.7	1
169	The longevity of subcontinental lithospheric mantle beneath Jiangsu-Anhui Region. Science in China Series D: Earth Sciences, 2001, 44, 1110-1118.	0.9	17
170	High-precision U-series dating of Holocene corals from South China Sea by thermal ionization mass spectrometry (TIMS). Science Bulletin, 1999, 44, 937-941.	1.7	9
171	Accretional History of the North and South China Blocks, and the Microcontinents Between them: Implications for Dispersion of Gondwanaland. Gondwana Research, 1999, 2, 585-588.	3.0	2
172	Os isotopic composition of the earth's primitive upper mantle. Science Bulletin, 1998, 43, 1575-1579.	1.7	4
173	Osmium isotope determination on mantle-derived peridotite xenoliths from Panshishan with N-TIMS. Science Bulletin, 1998, 43, 573-575.	1.7	13
174	Pb isotopes of granitoids suggest Devonian accretion of Yangtze (South China) craton to North China craton: Comment and Reply. Geology, 1998, 26, 859.	2.0	15
175	A Middle Silurian-Early Devonian Magmatic Arc in the Qinling Mountains of Central China: A Discussion. Journal of Geology, 1996, 104, 501-503.	0.7	43
176	Extracting 3D contour features of urban scenes from ground-based laser range data. , 0, , .		1
177	Shape similarities measures based on two-level ARG for the retrieval of remote sensing images. , 0, , .		0
178	A method of merging aerial images and ground laser scans. , 0, , .		1
179	In-situ experiments reveal mineralization details of porphyry copper deposits. Journal of Oceanology and Limnology, 0, , 1.	0.6	1
180	A New Video Stabilization Method for Airship Surveillance. , 0, , .		0

180 A New Video Stabilization Method for Airship Surveillance. , 0, , .

#	Article	IF	CITATIONS
181	Reworking of the Juvenile Crust in the Late Mesozoic in North Qinling, Central China. Journal of Earth Science (Wuhan, China), 0, , 1.	1.1	2
182	Chemical variations of loess from the Chinese Loess Plateau and its implications. International Geology Review, 0, , 1-16.	1.1	0